

We are IntechOpen, the world's leading publisher of Open Access books Built by scientists, for scientists

6,900

Open access books available

185,000

International authors and editors

200M

Downloads

Our authors are among the

154

Countries delivered to

TOP 1%

most cited scientists

12.2%

Contributors from top 500 universities



WEB OF SCIENCE™

Selection of our books indexed in the Book Citation Index
in Web of Science™ Core Collection (BKCI)

Interested in publishing with us?
Contact book.department@intechopen.com

Numbers displayed above are based on latest data collected.
For more information visit www.intechopen.com



A Tactile Sensing System Based on Arrays of Piezoelectric Polymer Transducers

Lucia Seminara, Luigi Pinna, Marco Capurro and Maurizio Valle

Additional information is available at the end of the chapter

<http://dx.doi.org/10.5772/50112>

1. Introduction

Tactile sensing enables robots to interact safely and effectively with unstructured environments and humans in case of both voluntary and reactive interaction tasks. Focusing on humanoid robots, there is increasing interest in avoiding negative human feelings towards the “entity” [1], enabling robots to interact with humans in more intuitive and meaningful ways [2-4]. This requires designing methods for extracting important information from tactile stimuli leading to classification of touch modalities [5-8]. It is still unclear, however, whether touch modality actually plays an important role in the communication of social messages. A very interesting research area consists in exploring social touch for robotics through an interpretation of emotions and other social messages [9].

Together with the social aspects of human-robot interactions, research in this field of robotics has focused largely on transduction principles and transduction technologies [10]. A survey of the state-of-the-art in robot tactile sensing is given by [11], with references to various sensor types. The functional requirements of a robotic skin remain debatable and are at least partially dependent on the specific application. However, some basic requirements can be identified. Sensors should be robust, stable, reproducible, showing a high sensitivity, capable of detecting a wide range of information and both static and dynamic touch (approximately in the 0 - 1 kHz frequency range). Moreover, this application demands mechanical flexibility and conformability, and the skin should be adaptable to various three-dimensional robotic platforms. Finally, the fabrication of the skin should be simple, low cost, replicable and scalable. All hardware should be portable and easily adaptable and electronics should be designed for minimum power consumption and minimum size.

Various technical issues have strongly limited the transition from small matrix prototypes to a large scale integrated solution. An example of truly scalable robot skin systems for humanoid robots has been proposed by Ohmura and Kuniyoshi [12]. They approached the

problem at system level introducing a networked architecture featuring peripheral nodes (chips) scanning (locally) a limited number of taxels. All the electronics and the transducers are embedded on a PCB support which allows a simple mechanical integration of the sensor over curved surfaces. However, the spatial resolution is quite low, and the adopted infrared (IR) optical transducers have quite large power consumption. The issue of fault tolerance, for infrared based sensors was previously addressed by Um and Lumelsky [13], who tackled the problem via component redundancy for a system featuring over 1000 sensing elements. Another example of artificial skin system for a humanoid robot has been proposed by Tajika et al. [14]. The sensor has been designed with the aim of detecting stimuli coming from people trying to interact with the robot and features PVDF based transducers, but the skin has low spatial resolution (the transducer area is of about 25 cm²).

At a high level, the goal of the ROBOSKIN European Project¹ is to develop and demonstrate a range of new robot capabilities based on the tactile feedback provided by a robotic skin from large areas of the robot body. To mimic the complex behavior of the human skin in a humanoid robot a multimodal system would be required, which employs different kinds of transducers. In particular, the present research is oriented to the development of distributed and modular components for general-purpose large-area tactile sensors based on piezoelectric polymer transducers. Piezoelectric sensors in the form of thin polymer films of Polyvinylidene Fluoride (PVDF) have been chosen [10,11,15-20], as they globally meet the given above sensor requirements except from perceiving static mechanical stimuli. Piezoelectric materials intrinsically convert the mechanical stimulus into an electrical signal on the basis of their electromechanical properties. The piezoelectric “functional” material must be integrated into structures which also include a substrate and a protective layer. How to integrate the PVDF transducer is not an easy task, because its response depends on several aspects including the properties of the whole mechanical chain, in particular material and thickness of the protective layer. Moreover, the design features also influence the requirements of the interface electronics and the data processing, to cite some of the most important aspects.

Following the system approach of the ROBOSKIN project, the research activities have been carried out by considering the skin as a system, which is as well a part of the overall robot architecture. Towards this perspective, a combined approach based on modelling and experimental testing is at the basis of the results achieved so far in the sensor manufacturing technology, the interface electronics, the tactile data processing, the embedded system architecture and the system integration. Main achievements in each of the cited fields will be outlined in this chapter.

The chapter will be organized as follows. To move towards an optimized design of the tactile sensing system, a preliminary experimental study has been carried out to classify the tactile stimuli in basic human-robot interactions. This aspect will be detailed in Section 2. The identified contact stress/force range has been used as reference for the design of the skin system.

¹ VII FP, <http://www.roboskin.eu>

In Section 3 attention will be focused on tactile sensing systems based on piezoelectric transducers. First, the electromechanical characterization of the *thickness-mode* behavior of piezoelectric polymer films will be presented. Therefore, first prototypes consisting in a single piezoelectric sensor covered by different protective elastomer layers will be described. Such prototypes have been employed both to validate the skin electromechanical model and to appropriately design the interface electronics., whose basic principles and circuits are reported in Section 4. A variable gain solution is also proposed to measure the wide range of tactile stimuli expected for the application.

The proposed skin system is made by conformable patches of triangular shape, interconnected in order to form a network structure [21]. Manufacturing and testing of triangular prototypes based on piezoelectric arrays are discussed in Section 5. Consequently, some system aspects related to prototype integration into the target robot platform, data transmission to the robot communication infrastructure and data processing requirements and algorithms are reported in Section 6. In relation to data processing, one of the goals of our research is the real-time implementation of tactile data processing by dedicated embedded digital circuits. In this view, an algorithm to provide the contact forces from sensor readings will be discussed.

An assessment of the achieved results and of the open issues paving the way for new research targets and novel design solutions will conclude the chapter.

2. From perception to tactile stimulus: human-robot interaction

A big challenge in robotics consists in designing a robot that is able to “feel,” “understand” and respond to touch in accord with human expectations. The human-like robot response to external stimuli is far beyond the scopes of this chapter, but a first step in this direction is to design a tactile sensing system which enables the robot to “effectively” interact with humans. This requires recognizing and classifying different *typical* modalities of touch. At a lower level, a first assessment of the expected dynamics of the tactile stimulus is needed, as a starting point to adequately design the interface electronics and the whole sensing system. This is the scope of this section.

More concretely, we have tried to quantify the magnitude of the mechanical stimuli involved in basic human-robot interactions. As we deal with piezoelectric transducers which do not perceive static stimuli, only impact forces have been considered. Basically, we aim at designing a tactile system which is able to measure and distinguish between light/tender touches and strong impacts.

To enable this quantitative study, a “modally tuned impulse force hammer” (PCB Piezotronics, Model 086C03) which is equipped with an integrated piezoelectric load cell has been used. The load cell acquires the temporal signal of an impact force, i.e. it measures the *effect* of an external force while impacting on another surface. A contact force is thus measured, which depends both on the hammer indenter and on the mechanical properties of the touched surface.

The idea is to associate a *perception* to a *quantification* of the tactile stimulus. Therefore, we reproduced with the hammer the elementary interactions listed in Table 1 on different areas of some candidate skin. Essays either on biological tissues (different hardness / different parts of the body, as specified) or on clothes have been performed. Among the different choices for the hammer indenter, the one has been chosen which was the most similar to a human finger. Another indenter with a plate shape has been used to simulate light / strong interactions with an open hand (caresses / slaps). This allowed us to find (at least partial) quantitative information about the external stimuli which are relevant for our application, in order to design the skin prototypes and the interface electronics.

To set the skin input stress range, maximum and minimum applied stimuli have to be quantified. To define those limits, the question is how to play with the involved variables, i.e. the indenter size/material and the material of the touched surface, in order to decide whether “force” or “pressure” is the meaningful quantity. The idea is to use “perception” as a definition criterion.

Contrary to our intuitive understanding based on personal experience, the brain is not a camera that passively records the external world. Perception is a product of the brain's abstraction and elaboration of sensory input. The somatic sensory system transmits information about four major modalities: touch, proprioception, pain, and temperature sense. The four modalities are conveyed in separate ascending pathways to the thalamus and cerebral cortex. The perception of touch or pressure is consistent when touch-pressure receptors are electrically stimulated [22].

When touching the human skin, upper limits for the mechanical stimulus can be considered those associated with a “pain” feeling. Pain is, of course, a sub-modality of somatic sensation like touch, pressure, and position sense and serves as an important protective function. It is a complex perception. Its highly individual and subjective nature is one of the factors which makes it difficult to define and to treat clinically. More than any other sensory modality it is influenced by emotional state and environmental contingencies. Therefore, the same stimulus can produce different responses in different individuals under similar conditions. However, average behaviors are interesting in this context and the pain feeling can be used to approximately identify the stimulus upper limit. In particular, when testing different hardness indenters on different parts of the body, we observed that pain limits the maximum stress. The *maximum force* can be determined on the basis of the contact surface. The lower limit is on the contrary determined by the minimum perceived force. In this case *force* seems to be the relevant parameter and the *minimum stress* is thus calculated using the largest employed contact surface, approximately corresponding to a human hand.

Given the considerations above, the maximum stress corresponds to approximately 5.5 MPa, which corresponds to a force of 120-130 N (small indenter radius equal to 2.7 mm). On the other hand, to quantify the smallest force we used the PLATE-like indenter (radius equal to 35 mm), and the value we found is $F = 0.2$ N, which corresponds to approximately 50 Pa. Therefore, the application range goes from 50 Pa to 5 MPa (over 5 orders of magnitude). Moreover, the stiffness difference in various skin areas seems to influence the measured

contact force by a factor of approximately 3-4, with softer samples producing lower amplitudes. Results are summarized in Table 1.

TYPE of interaction	CONTACT FORCE (N)	PRESSURE (MPa)	Employed contacting tools	Contact DIAMETER (mm)	TESTED zones (different hardness, different sensitivity)	Impact type
Poke / finger mark	0.2 - 1.4	0.016 - 0.11	SOFT SPHERICAL INDENTER	4	Cheek, arm, belly (SOFT); shinbone, knee, back (HARD)	LIGHT
Poke / finger mark	20 - 130	0.86 - 5.6	SOFT SPHERICAL INDENTER	5,45	Thigh, Cheek, forearm, belly (SOFT); cheekbone, knee, back (HARD)	HARD
Light touch / caress	0.2 - 1.4	$5.2 \cdot 10^{-5}$ - $3.6 \cdot 10^{-4}$	BIG PLATE	70	Cheek, belly (SOFT); back (HARD)	SUPER SOFT
Smack / slap	70 - 170	0.018 - 0.044	BIG PLATE	70	Cheek, belly (SOFT); back (HARD)	HARD

Table 1. Basic human-robot interactions (impacts).

Our results are in accordance with literature, where typical human interactions are basically considered to range from approximately 1 N for a soft stroke up to approximately 100 N for a push or slap. In a recent paper published on Nature Materials [23], authors state that normal manipulation tasks involve stresses of the order of 10-100 kPa, while gentle touches correspond to stress values which are lower than 10 kPa.

We also compared our estimations with the specifications of commercial products which are today on the market, i.e. the Barrett hand² and BioTAC³. The Barrett Hand has a sensor resolution which is a bit lower (but of compatible order of magnitude on the palm) with respect to the smallest forces the application would require, and which correspond to 660Pa on fingertips, 330 Pa on fingers and 200 Pa on the palm. As regards the BioTAC Multimodal Biomimetic Tactile Sensor, a typical 0.03 N to 30 N force dynamic range is guaranteed, which is again compatible with the proposed dynamics which has been given in terms of the more appropriate *pressure* parameter (considering different contact areas). These are commercial products and specifications are related to *manipulation* tasks, however such data can be used as an indicative benchmark.

² http://www.barrett.com/robot/DS_BarretHand.pdf

³ <http://www.syntouchllc.com/TechSpecSheet.pdf>

3. Assessment of the skin behavior

3.1. Electromechanical characterization of PVDF films

Commercial 100 μm thick PVDF sheets from Measurement Specialties Inc.⁴ have been purchased. PVDF samples have been cut from those sheets in a square geometry of 7x7 mm². Purchased sheets have been already stretched and poled. The process begins with the melt extrusion of the polymer resin pellets into sheet form, followed by a stretching step that reduces the sheet to about one-fifth its extruded thickness. Stretching at temperatures well below the melting point of the polymer causes chain packing of the molecules into parallel crystal planes (beta phase). The beta phase polymer is poled by application of very high electric fields (of the order of 100 V/ μm) to align the crystallites to the poling field. In such conditions the piezoelectric film exhibits a material symmetry in the orthorhombic crystal system (C2V class), corresponding to that of the so-called orthotropic materials. The samples are oriented with axis 1 along the stretching direction – axis 2 in the in-plane orthogonal direction and axis 3 along the through-thickness direction (see Figure 1).

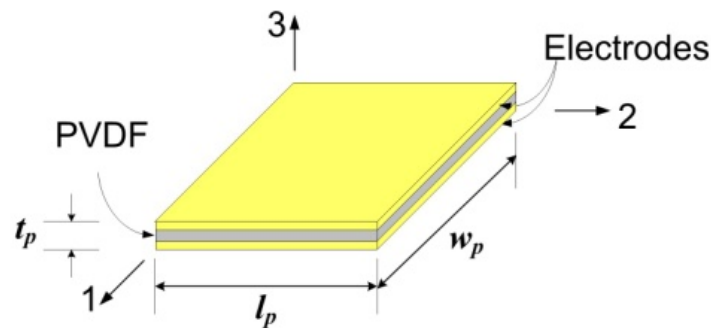


Figure 1. PVDF provided of electrodes to extract the charge signal. Reference axes are shown.

Linear electro-elastic constitutive equations are commonly used to describe the coupling of dielectric, elastic, and piezoelectric properties in piezoelectric materials [24].

In the frequency domain ($\hat{f}(\omega)$) means the Fourier Transform of any function ($f(t)$) such equations are:

$$\begin{bmatrix} \hat{S} \\ \hat{D} \end{bmatrix} = \begin{bmatrix} \hat{s} & \hat{d}^T \\ \hat{d} & \hat{\epsilon} \end{bmatrix} \begin{bmatrix} \hat{T} \\ \hat{E} \end{bmatrix} \quad (1)$$

where strain \hat{S} and stress \hat{T} are represented by 1x6 column vectors, while the electric displacement \hat{D} and the electric field \hat{E} are expressed by 1x3 column vectors. \hat{s} is the 6x6 compliance matrix, $\hat{\epsilon}$ the 3x3 permittivity matrix, both assumed to be symmetric, and \hat{d} the piezoelectric 3x6 matrix.

In our application, the PVDF behavior is usefully described by the second row of constitutive equations:

⁴ <http://www.meas-spec.com/default.aspx>

$$\begin{bmatrix} \hat{D}_1 \\ \hat{D}_2 \\ \hat{D}_3 \end{bmatrix} = \begin{bmatrix} 0 & 0 & 0 & 0 & \hat{d}_{15} & 0 \\ 0 & 0 & 0 & \hat{d}_{24} & 0 & 0 \\ \hat{d}_{31} & \hat{d}_{32} & \hat{d}_{33} & 0 & 0 & 0 \end{bmatrix} \begin{bmatrix} \hat{T}_{11} \\ \hat{T}_{22} \\ \hat{T}_{33} \\ \hat{T}_{23} \\ \hat{T}_{13} \\ \hat{T}_{12} \end{bmatrix} + \begin{bmatrix} \varepsilon_{11} & 0 & 0 \\ 0 & \varepsilon_{22} & 0 \\ 0 & 0 & \varepsilon_{33} \end{bmatrix} \begin{bmatrix} \hat{E}_1 \\ \hat{E}_2 \\ \hat{E}_3 \end{bmatrix} \quad (2)$$

The structures of the piezoelectric and the permittivity matrices are due to the reported material symmetry.

As the charge signal is measured with a charge amplifier, which converts the charge input into a voltage without supplying any electric field, the electric field can be set to null. Therefore, when the film is used in *thickness mode* the previous set of equations reduces to:

$$\hat{D}_3 = \hat{d}_{33} \hat{T}_{33} \quad (3)$$

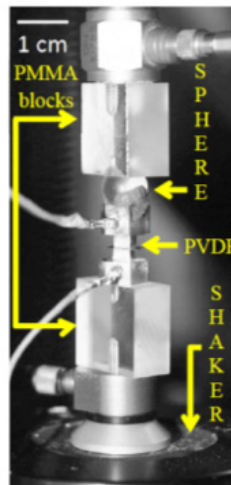


Figure 2. Compression test setup to measure the d_{33} coefficient.

For the present application, characterizing the electromechanical behavior of the piezoelectric polymer means to retrieve the frequency behavior of the d_{33} piezoelectric coefficient.

The employed experimental equipment has been thoroughly discussed in a previous publication [25], which reports more complete characterization results of the PVDF electromechanical behavior. Briefly, the experimental setup (see Figure 2) consists of a rigid frame with a lower fixed plate to which an electro-mechanical shaker is assembled. A piezoelectric force transducer is fixed to the upper head of the frame. Samples are mounted between the force transducer and the shaker. They are pressed between two metals heads of square cross-section with machined and polished contact surfaces. The lower head is assembled to the shaker head with an interposed PMMA block, and the upper head contrasts through a spherical joint with a similar block connected to the force transducer, for

self-alignment of the contact planes. Conductive glue creates a stiff connection between the sample and the heads thus excluding possible variations in the contact area during measurements.

The test is controlled by a computer in a completely automatic way. A swept sine signal is fed into the shaker. Frequency spacing and total duration of the test are determined by the settable frequency range and number of steps. The output charge signals (response) and force transducer (stimulus) are continuously acquired and processed in frequency to give the complex piezoelectric modulus. Normally the range between 10 and 1000 Hz can be explored without difficulties.

The frequency behavior of the d_{33} piezoelectric coefficient is shown in Figure 3. The most relevant result in this context is the almost flat behavior of both the real and imaginary parts of the modulus in the considered frequency range, in accordance with literature [26].

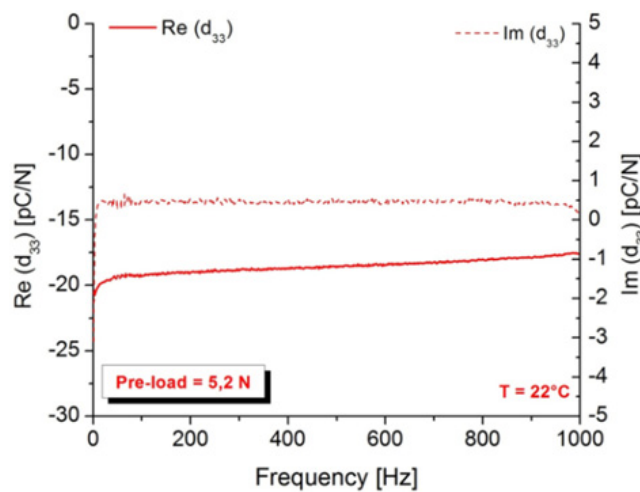


Figure 3. Frequency behavior of the real and imaginary parts of the d_{33} piezoelectric coefficient.

3.2. Electromechanical modeling of the skin structure

In order to associate the PVDF charge response to the effective load applied on the outer skin surface, a skin model which is based on the Boussinesq's equation has been considered.

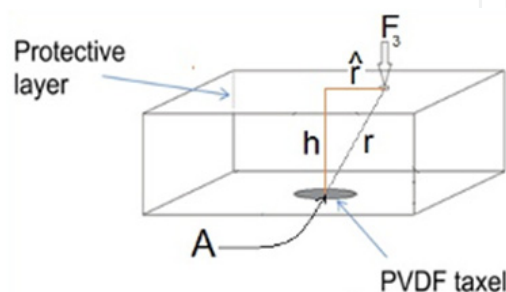


Figure 4. The PVDF sensor is located at the bottom of the protective layer of thickness h and a point force is applied on the outer surface.

Approximately, the relation between a point load \mathbf{F} applied on the outer surface and the stress at a given point inside the cover layer is given by the Boussinesq's equation [27]:

$$\mathbf{T} = \frac{3}{2\pi} \frac{\mathbf{F} \cdot \mathbf{e}_r}{r^2} \mathbf{e}_r \otimes \mathbf{e}_r \quad (4)$$

where all bold faced symbols represent tensors or vectors, \mathbf{e}_k is the unit vector in the k -direction and \otimes is the symbol of the tensor product. The Boussinesq's problem considers a linearly elastic half-medium on which a point force is applied. Truly, the materials employed in the present application (typically elastomers or gels) are both non-linear elastic and visco-elastic. Nevertheless, Equation (4) does not depend on the elastic modulus and deviations from linearity are only expected as a consequence of geometry changes due to large deformations. For the applicability of the model, therefore, a sufficiently rigid protective layer should be chosen. In addition, Equation (4) holds whenever the Poisson ratio of the medium is close to 0.5. This holds for an elastomer ($\nu = 0.48$), but not for other materials (e.g. a foam). A complete solution valid for all ν is available in [28], but it is considerably more complex. The major approximation concerns the finite thickness of the layer, compared with the semi-infinite medium. The advantage of (4) is its simplicity, as the stress is uniaxial in the radial direction, and its independence of elastic parameters.

Equation (4) is applied to a sensor located on the bottom of the elastic cover of thickness h . The sensor works in the thickness mode, i.e. it can read the T_3 stress component ('3' is the direction normal to the bottom surface) via the d_{33} piezoelectric modulus. Letting \hat{r} be the radial distance of the point where the force is applied from the sensor center projected on the outer surface, we have $r^2 = \hat{r}^2 + h^2$ and $\mathbf{e}_r = \sin\theta(\mathbf{e}_1 \cos\varphi + \mathbf{e}_2 \sin\varphi) - \mathbf{e}_3 \cos\theta$, where $\sin\theta = \hat{r}/r$.

Then we obtain:

$$T_3 = \frac{3}{2\pi} \frac{h^2}{(\hat{r}^2 + h^2)^{5/2}} \{ (F_1 \cos\varphi + F_2 \sin\varphi) \hat{r} - F_3 h \} \quad (5)$$

For a vertical force ($F_1 = F_2 = 0$) Equation (5) reduces to:

$$T_3 = -\frac{3}{2\pi} \frac{F_3 h^3}{(\hat{r}^2 + h^2)^{5/2}} \quad (6)$$

As T_3 is related to the charge density D_3 on the sensor surface by the piezoelectric constitutive equation:

$$D_3 = d_{33} T_3 \quad (7)$$

under the hypotheses that the sensor size is sufficiently smaller than its distance from the point force, the total charge measured by the sensor can be approximated by:

$$q = -\frac{3}{2\pi} A \frac{d_{33} F_3 h^3}{(\hat{r}^2 + h^2)^{5/2}} \quad (8)$$

3.3. Experimental assessment of the single taxel behavior

In order to optimize the design of the skin prototypes we checked the pertinence/limits of the mechanical model, thus quantifying the PVDF electrical response to the external mechanical stimuli and testing the effect of the protective layer (material and thickness) on the PVDF response. We performed the tests on basic single taxel prototypes, where a single circular PVDF film is covered with an elastomeric cover to protect the sensor from physical damage by shocks or chemical contamination by oil and other materials. Attention has been focused on gel/rubber layers, in that they are more controllable and reproducible systems which also allowed for the required dynamics.

An experimental campaign has been carried out in order to quantify the sensor output charge in common tactile interaction tasks. The mechanical input stimuli range from 50 Pa to 5 MPa, as reported in section 2.

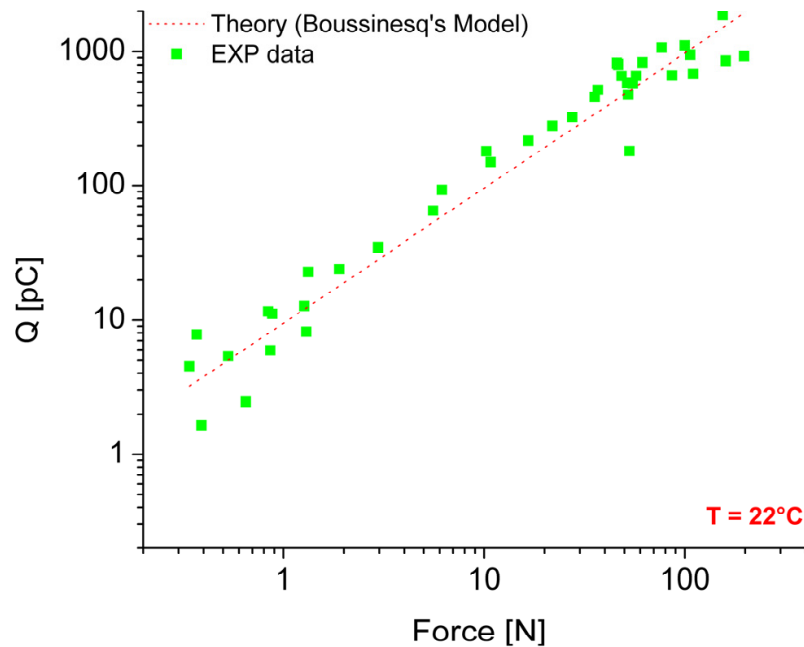


Figure 5. Single taxel skin prototype: comparison between model and experiments.

The “modally tuned impulse force hammer” (see Section 2) has been used to mechanically stimulate the single taxel sample. In this case, we recall that the load cell measures a contact force, which depends both on the indenter and on the protective layer materials. The measured charge over the 5 kPa - 5 MPa stress range has been compared with the model presented in the previous section and results are reported in Figure 5. In this case, on the horizontal axis the peak amplitude of the *time behavior* of the contact force is reported. Similarly, the peak amplitude of the charge response is reported on the y axis. It is

important to remark here that these measurements are not at all easy to perform, as it is not yet possible to accurately control the position of the hammer impact. A good statistics would be thus required to achieve reliable results. Results are however useful to understand the “order of magnitude” of the charge response and the limits of applicability of the models.

A good accordance between model and experimental data is recorded for high loads, which allows extending the model linear behavior for lower loads, thus covering the whole stress range which is of interest for the application (50Pa - 5MPa). Therefore, both charge and force ranges cover 5 orders of magnitude, the typical output charge ranging from 0.01 pC to 1 nC. This information has been a reference point for the design of the electronics.

4. Interface electronics

In Figure 6 the basic block diagram of the interface electronics is shown. The interface electronics converts the charge developed by the PVDF – as a result of the applied stress – to a voltage signal. It includes a Charge Amplifier (CA) cascaded with a Low Pass Filter (LPF) with high *cutoff frequency*, f_H . The CA has a high pass response with low *cutoff frequency*, f_L . The frequency band of interest at constant gain is, therefore, defined as $BW = f_H - f_L$.

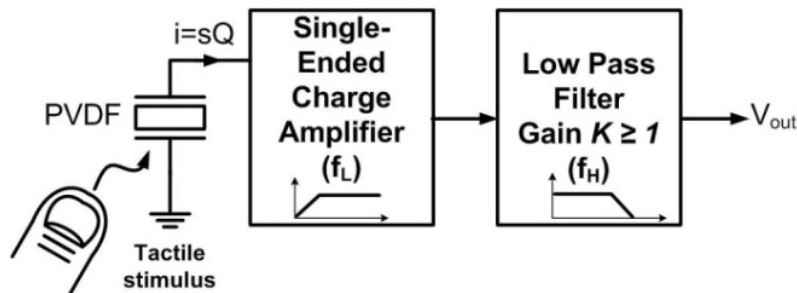


Figure 6. Basic block diagram of the interface electronics.

The mathematical expression of the charge generated by the PVDF sensor can be found from the piezoelectric constitutive equation (2) of Section 3.1. Considering the op amp as ideal, the electric field E_3 across the PVDF sensor is negligible because of the virtual ground at the op amp non inverting terminal. Therefore, under the assumption of the thickness mode operation, the expression for the electrical displacement reduces to (3). The charge generated by the PVDF sensor can be found by integrating the electrical displacement D_3 over the loading area A_c :

$$q = \iint_{A_c} D_3 dA_3 = d_{33} A_c T_3 = d_{33} F_c \quad (9)$$

where the stress $T_3 = F_c / A_c$ is assumed to be uniform over the loading area, and F_c is the applied contact force (see Figure 7).

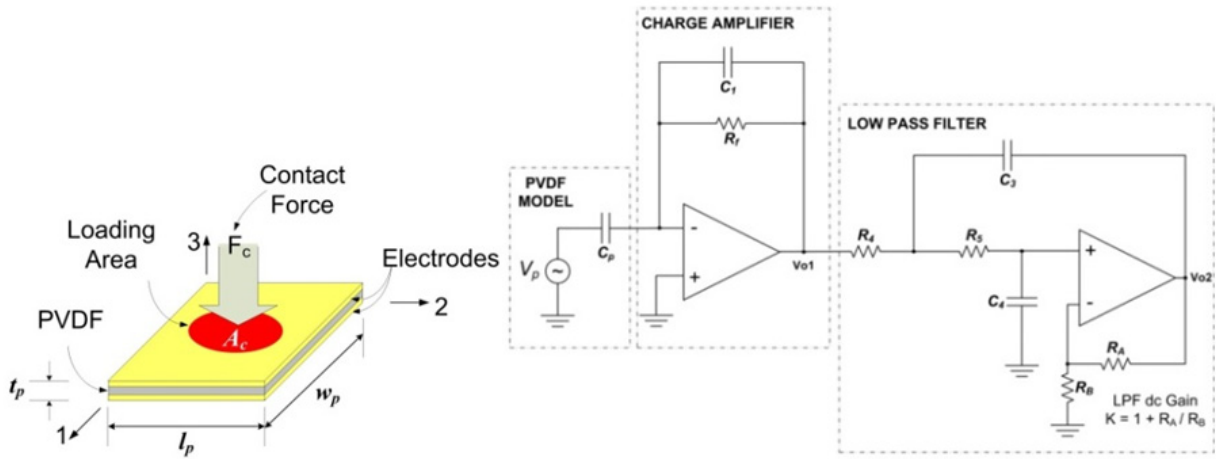


Figure 7. PVDF tactile sensor: The PVDF material (in the middle) is provided of two electrodes (left). Charge amplifier connected to the PVDF equivalent electrical circuit model and the cascaded low pass filter (right).

Figure 7 (right) shows the simplified equivalent circuit model of the PVDF sensor connected to the CA. In order to find the mathematical expression for the equivalent voltage source V_p Equation (2) can be used. In case of open circuit across the electrodes of the PVDF film, D_3 is zero. Therefore, expressing the electric field as the ratio of the open circuit voltage to the PVDF thickness (i.e. $E_3 = V_p/t_p$) and considering the loading area A_c equal to the PVDF area A_{PVDF} , we found:

$$V_p = -\left(\frac{t_p}{\epsilon_{33}A_c}\right)d_{33}F_c = -\frac{q}{C_p} \tag{10}$$

where $C_p (= \epsilon_{33}A_{PVDF}/t_p)$ is the equivalent capacitance of the PVDF film and $q (= d_{33}F_c)$ is the resulting charge. Using (10) and by analyzing the circuit of Figure 7 (right), the transfer function of the CA – in terms of the input charge to the output voltage ratio – can be found:

$$H_{CA}(s) = \frac{V_{o1}}{q} = \frac{sR_f}{1 + sC_1R_f} \tag{11}$$

The sensitivity of the CA is given by the ratio between the maximum output voltage (i.e. the supply voltage in the ideal case) to the maximum input charge. The sensitivity sets the value to be given to the feedback capacitance C_1 (i.e. $V_{o1,max} / q_{max} = 1/C_1$). Moreover, the CA low cutoff frequency defines the value to be given to the feedback resistance R_f (i.e. $f_L = 1/(2\pi R_f C_1)$).

4.1. Effects of the operational amplifier non idealities

The objective of the present section is to analyze the limitations which come into play when the op amp non idealities are taken into account. The non-idealities influence the behavior both of the op amp and of the PVDF tactile sensor.

4.1.1. Finite op amp open-loop gain

The open-loop gain of an op amp, a , is not infinite, therefore, the electric field, E_3 across the electrodes of the PVDF is not negligible. Hence, the dielectric contribution due to the electric field cannot be neglected in the piezoelectric constitutive Equation (2). Therefore, the total charge in input to the CA, is:

$$q_{tot} = (d_{33}F_3) + \left(-\frac{\epsilon_{33}A_{PVDF}}{t_p} \frac{V_{o1}}{a} \right) = q_F + q_E \quad (12)$$

where the first term q_F is due to the applied force (i.e. direct piezoelectric effect), while, the second term q_E is due to the electric field caused by the op amp finite open-loop gain (i.e. inverse piezoelectric effect).

Component Name	Value	Unit
$a^{(b)}$	10^6 (120dB)	V/V
C_1	100	pF
C_3	2.7	nF
C_4	1	nF
R_1	100	M Ω
R_2	9	k Ω
R_3	1	k Ω
R_4	3.6	k Ω
R_5	7.5	k Ω
$R_A^{(b)}$	N.A.	Ω
$R_B^{(b)}$	N.A.	Ω

^(a) The LPF has a unity gain

^(b) Open-loop gain OPA703

Table 2. Charge amplifier and low pass filter component values.

In order to quantify how the finite open-loop gain could contribute to the generated charge let us give the following example. Let the op amp be the OPA703⁵ which is supplied at ± 5 V. The CA parameters are the ones reported in Table 2; let the range of contact forces be 0.1 N \div 25 N (where the maximum force makes the CA output to saturate to 5 V); and let us assume $A_{PVDF} = Ac$. Finally, let the PVDF parameters be the ones reported in Table 3. Using Equation (12) the charge contribution due to the op amp finite open-loop gain is reported in Table 4.

⁵ <http://www.ti.com/lit/ds/symlink/opa703.pdf>

As it can be seen from the values reported in Table 4, the charge, q_E due to the electric field contribution can be considered negligible, with respect to the dielectric contribution, the higher the op amp open-loop gain is.

Name	Parameter	Value	Unit
Piezoelectric constant ^(a)	d_{33}	-20	pC/N
Permittivity ^(a)	ϵ	106	pF/m
Relative permittivity ^(a)	ϵ_r	12	
PVDF thin film Length	l_p	5	mm
PVDF thin film Width	b_p	5	mm
PVDF thin film Thickness ^(a)	t_p	110	μm
PVDF electrode surface ^(b)	$A_{PVDF}=A_e = b_p \cdot l_p$	25e-6	m ²
Static Capacitance ^(b)	$C_p = (\epsilon_{33} A_c)/t_p$	24	pF
Input charge	$q = d_{33} F_c$	0.2 ($F_c = 0.01\text{N}$) \div 500 ($F_c = 25\text{N}$)	pC
Equivalent PVDF voltage source	$V_p = -q/[(\epsilon_{33} A_c)/t_p]$	2e-3 ($F_c = 0.01\text{N}$) \div 5 ($F_c = 25\text{N}$)	V

^(a) Piezo Film Sensor Technical Manual, Measurement Specialties, Inc.

^(b) Refer to Figure 7.

Table 3. PVDF parameters.

F_c [N]	q_F [pC]	q_E [pC]
0.01	-2	-48.2e-9
25	-500	-120 e-9

Table 4. Contribution of the op amp finite open-loop gain to the input charge.

Moreover, if we consider the finite op amp open-loop gain, the CA frequency response becomes:

$$A_{CA,q}(j\omega) = \left(\frac{a}{1+a} \right) \left(\frac{t_p}{\epsilon_{33} A_c} \right) \left[\frac{j\omega C_p R_f}{1 + j\omega \left(\frac{a}{1+a} \right) R_f \left(C_1 + \frac{C_1 + C_p}{a} \right)} \right] \quad (13)$$

The module of (13) at low frequency tends to zero, while for high frequencies, it tends to:

$$|A_{CA,q}(j\omega)| \cong \left(\frac{t_p}{\epsilon_{33} A_c} \right) \frac{C_p}{\left(C_1 + \frac{C_1 + C_p}{a} \right)} \quad (14)$$

For high values of the op amp finite open-loop gain the term $(C_1+C_p)/a$ of Equation (14) becomes negligible.

The influence of the finite op amp open-loop gain can be considered negligible both as contribution to the generated charge and as contribution to the output frequency response of the CA. Therefore, for the analysis the op amp can be approximately considered as ideal.

4.1.2. Finite Gain-bandwidth product (GBP)

The gain-bandwidth product (GBP) defines the limit of the op amp amplification, introducing a *cutoff frequency* at high frequency. When choosing an op amp it is worth to check accurately if the op amp has a GBP that allows the CA to achieve the target pass-band frequency range. Table 5 reports the results of the comparison among the three op amps which have been chosen for their suitable features in terms of GBP, open-loop gain, supply voltage and package size for the design of the interface electronics.

Both the package size and supply voltage are two important specs to be considered because of the small space available on the robot. In fact, the use of single supply op amps allows reducing the number of components without degrading the circuit performance – negative voltage regulators are not necessary thus reducing the required number of components. Components with small packages should be preferred to save space. Therefore, according to the considered op amp specs summarized in Table 5 the OPA347 is the better tradeoff.

		OPA703	OPA347*	OPA348†
GBP		1 MHz	350 kHz	1 MHz
Open-loop gain		120 dB	115 dB	108 dB
Supply voltage		Double/Single ±2V to ±6V 4V to 12V	Single +2.3V to +5.5V	Single +2.1V to +5.5V
Package	Type	SOT23-8 SO-8	WCSP-8	SOT23-8 SO-8
	Size (mm)	W x L x H 2.8x2.9x1.45	W x L x H 2x1x0.625	W x L x H 2.8x2.9x1.45

*<http://www.ti.com/lit/ds/symlink/opa2347.pdf>

†<http://www.ti.com/lit/ds/symlink/opa348.pdf>

Table 5. Comparison among some off-the-shelf op amps characteristics in terms of GBP, supply voltage and package size.

Figure 8 shows that op amps in Table 5 satisfy the $1 \text{ Hz} \div 1 \text{ kHz}$ bandwidth specification for the *frequency band of interest*.

The experimental results validate the proposed circuit approach. The behaviour of the interface electronics is linear in the given frequency range. The input signal range of the interface electronics was able to measure up to 3 orders of input force magnitude range. In order to extend the input range of the detectable signal up to the 5 orders of magnitude expected for the application, a variable gain amplifier is currently under development.

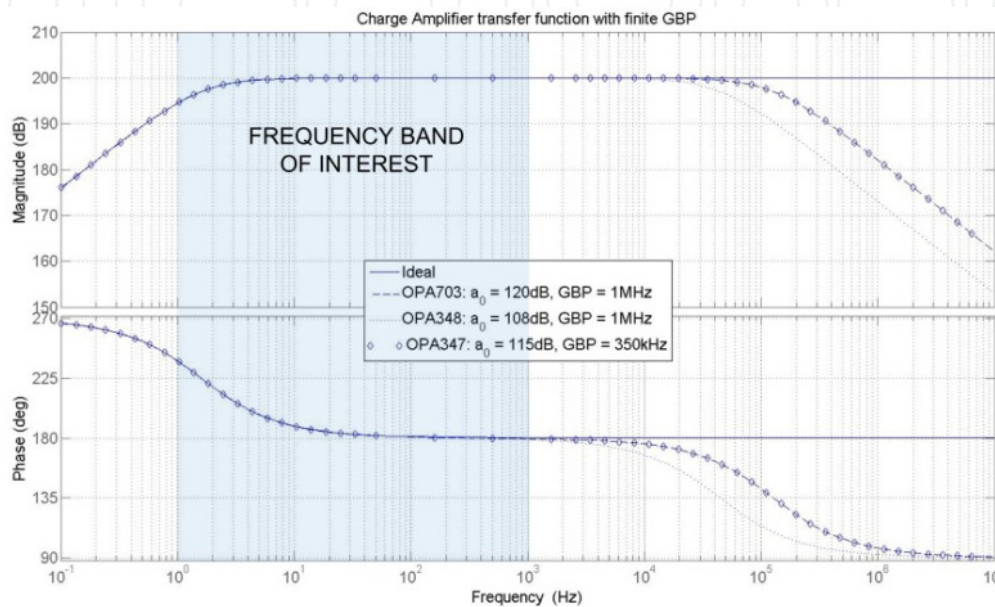


Figure 8. Comparison between the ideal and CA frequency responses using an ideal op amp, the OPA703 and the OPA348/7 with their corresponding finite GBPs.

5. Skin technology and experimental results

The basic structure of skin prototypes based on PVDF arrays is reported in Figure 9. Piezoelectric sensors have to be integrated on a rigid substrate and an elastomer layer is integrated on top as protective layer. This section briefly describes the technological solutions adopted to assemble the different building blocks. Details will be contained in a forthcoming publication.

The triangular geometry, taxel size and positions have been chosen to reproduce existing conformable skin patches manufactured at IIT (Italian Institute of Technology, Genoa) and based on capacitive transducers (*Roboskin project*).

Among technology solutions, how to provide PVDF films with metal contacts is a crucial point. Although metalized PVDF is commercially available, the brittleness of some of the available coatings (Copper over nickel, aluminum on chrome), the high roughness of the screen-printed silver ink solution and the impossibility of obtaining - as a prototyping service - custom patterning of the conducting film from the suppliers, convinced us that operating a “home-made” metallization was a better choice. We thus purchased *bare* piezoelectric polymer foils and made ad-hoc electrodes employing inkjet deposition technologies.

A whole metal layer (common ground) is deposited on top of the PVDF film, while patterned contacts with the same geometry of metal contacts on PCB (Figure 9) are deposited on the PVDF bottom side. Conductive glue has been used to fix the PVDF film on the PCB. The cover lay avoids short-circuits between taxels due to the employed glue. The protective layer is finally integrated on top. A Two-part silicone Sylgard® 184 Silicone Elastomer (*Dow Corning*) that cures to a flexible elastomer (PDMS) has been employed and it is directly polymerized on the PCB. Adhesion between PDMS and PVDF has been increased by the use of an *adhesion promoter*. A 2,5mm thick layer has been finally chosen as optimally meeting the application requirements.

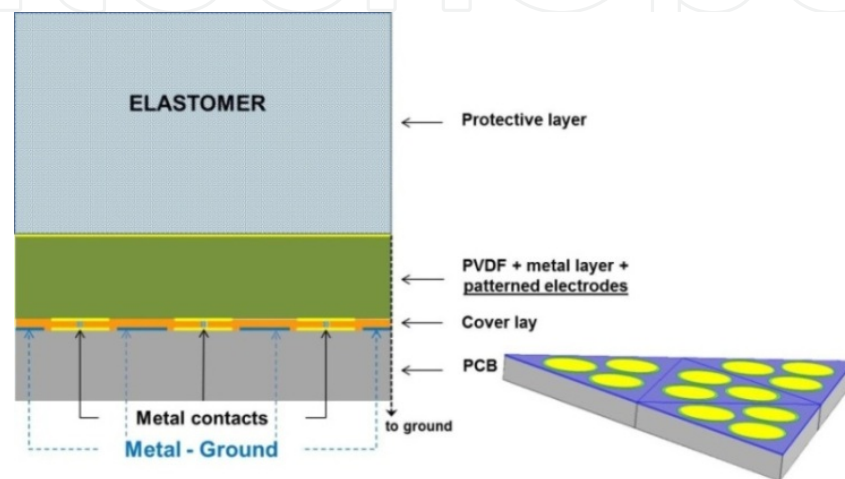


Figure 9. Structure of skin prototypes based on piezoelectric polymer arrays.

Figure 10 shows some results of experimental tests on triangular prototypes. A sinusoidal mechanical stimulus has been applied in correspondence of a certain taxel, by means of an indenter stiffly connected to an electromechanical shaker.

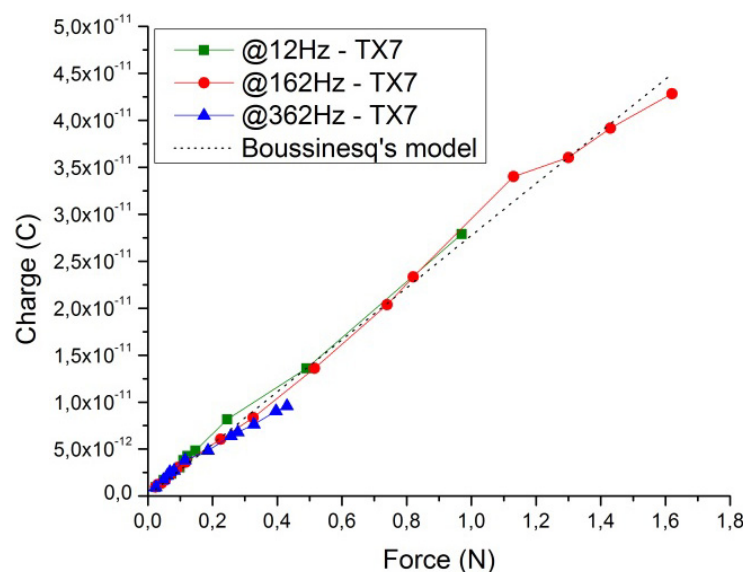


Figure 10. Comparison between experimental data at different frequencies and Boussinesq's model. Mean of peak values of sinusoidal waveforms at different frequencies are shown.

The tests have been conducted by varying the amplitude of the input force for different frequency values. Figure 10 shows the measured charge at 12 Hz, 162 Hz and 362 Hz compared with the value obtained using the Boussinesq's equation (see Section 3.2). As it can be seen a good correspondence can be found. A good linearity is achieved over the whole explored range, and the same voltage-to-force behavior for different frequencies is recorded (in accordance with d_{33} results reported in Section 3.1).

6. Towards system integration

6.1. Data processing

As for humans the cerebral cortex constructs an image of touched objects from the fragmented information provided by skin receptors, in a similar way tactile data processing is needed to enable the robot response to external stimuli. Starting from sensor data, the development of methods for touch interpretation is not an easy task.

Towards this scope, this chapter presents the basic ideas of a *force reconstruction* algorithm. The tactile stimuli applied on the outer surface of the elastomer and filtered by the soft layer, are assumed to be received by the sensors as stress components. Any tactile recognition task is haunted by the following problem: given the output of the sensor array, derive the force distribution on the outer surface. The problem is fatally an ill-posed one: in fact the set of the data is discrete (the sensor number is finite) and the set of the unknowns is a continuum (a force distribution is a vector field).

The proposed model exploits a discretization of the original continuous problem by constructing an array of concentrated forces at discrete points on the skin surface, starting from the information provided by the sensor array (normal stress measurements).

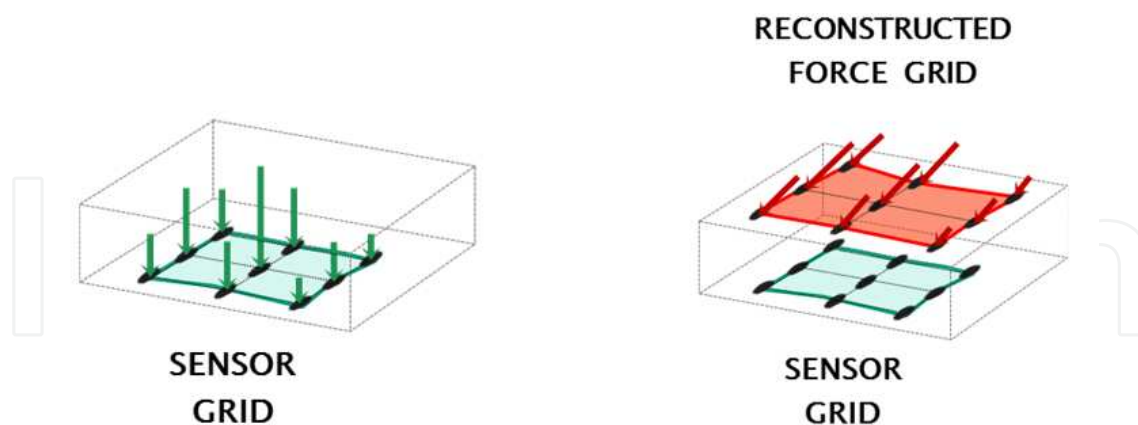


Figure 11. (a) A distribution of forces (not shown in the figure) acts on the cover layer. The pure normal stress component is recorded by the sensor array which is located beneath the elastomer layer. (b) From the sensor electrical outputs - through the developed algorithm - the force is reconstructed at discrete points over the outer layer.

If the force distribution is discretized into an array of point forces, a superposition of the Boussinesq equations (Section 3.1) for the single point forces can be used as a particularly simple and attractive approximation in the case of linear elasticity.

Mathematically it reduces to a linear vector equation $b = Cx$, where C is in general a rectangular matrix. The discretized problem consists in solving this equation for the force vector x .

The inverse Boussinesq's problem has a direct and unique solution only if C is a square full-rank matrix. This would imply that the number of sensor outputs is the same as the number of force components. If we have one output per sensor (typically, the normal stress) and want to explore 3-component surface forces, the number of points in the force array should be one third of that in the sensor array, to meet the condition. Such a solution would be rather poor in definition.

We examined a solution where the number of point forces (applied to the nodes of a pre-determined grid) is equal to the number of sensors. Initial assumptions are made (some can be relaxed in further developments) in that the problem is considered to be static, the surface plane, deflections are small and the elastomer layer Poisson ratio close to 0.5. The method consists in creating a series of x solutions – written as a function of two scalar parameters - to the ill-posed problem. Those are built by using the Moore-Penrose pseudo inverse matrix [29] and an orthogonal projector acting on a not completely defined w vector which, however, fulfills the essential physical constraints (for instance, in a contact problem compressive normal forces and horizontal forces in the friction cone are expected). The eligible solution is the one which minimizes a cost functional corresponding to the norm of the difference between the generic x solution and the w vector.

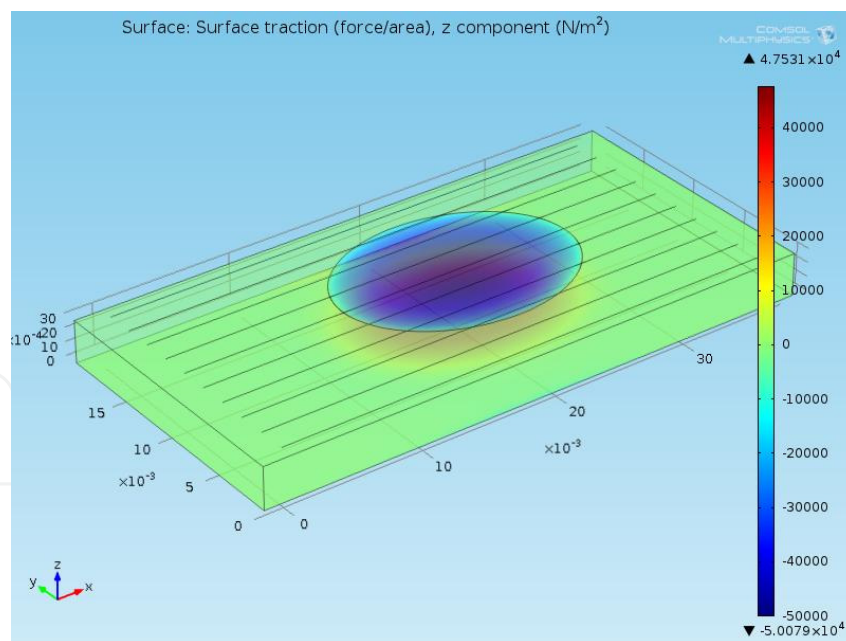


Figure 12. 3D representation of the test case, with only the normal traction field evidenced.

A check of the algorithm was made in MATLAB on a modeled skin structure consisting in a rectangular patch 40×20 mm² in size with a 10×10 point-like sensor grid at the bottom and 3mm thick elastomer layer (Figure 12). An hertzian force distribution with normal and tangential components (directed at 45° to the longitudinal axis of the patch) was applied to

an elliptical area on the outer surface. The model was previously evaluated by a FEM computation and the normal stress at the center of each sensor was calculated.

The algorithm described above has been applied to retrieve the 3 traction components on the loading area, having the sensor stress values as inputs (b vector). The result concerning the sole normal component is shown in Figure 13.

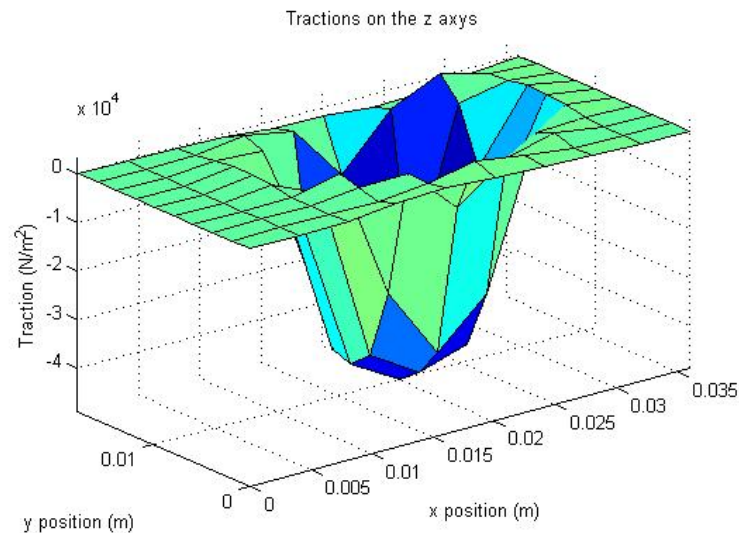


Figure 13. Algorithm output: normal traction on the outer surface.

The shape of the distribution as well as its peak value appears to be in very good accord with the assigned data. The tangential components, which are not shown in the present context, can be also retrieved within a certain approximation.

A crucial feature of the present research is that the proposed algorithm should be efficiently implemented on digital hardware. This in turn allows for real-time implementation of tactile data processing into embedded electronics systems.

In a wider perspective, this work is intended as a first step towards the integration of different techniques for tactile information processing (e.g. computational intelligence), possibly implemented at different levels of the transmission line towards the robot central processor. In its difference from statistical approaches such as Machine Learning, the advantage of the present algorithm is that it does not require time-consuming training and data set analysis.

6.2. System architecture

A robot skin can be seen as a complex system formed by a large number of spatially distributed sensing elements with embedded local processing electronics [30]. The robotic

skin should be designed in order to be independent from and compliant to different robotic platforms. Small/large scale-tailor-made robotic skin could require different transduction principles (capacitive, piezoelectric, etc.) for the multimodal transduction of contact features.

The robot skin design should focus on the following topics:

- Robot skin as a system. The Robot skin is intended to be a set of flexible or curved and compliant patches covering a large area of the robot body. Each patch is composed of a given set of tactile sensing arrays (i.e. 2-D arrays of taxels) and of embedded and dedicated electronics. Patches can be interconnected and networked to each other in order to achieve large sensing surfaces, where contacts or interactions are mostly expected to happen.
- Robot skin as a sensor. The tactile sensor is intended to be multimodal and it should include detection and measurement capabilities (i.e. contact event, force distributions, temperature, etc.).
- Robot skin electronics. Development of large parts of robot skin with a modular approach: i.e. configuring robot skin parts as the functional, electrical and mechanical aggregation of basic tactile sensing arrays with dedicated and embedded interface electronics, local data acquisition and processing. Each module will be networked with the others in order to configure scalable and modular arrangements.

Despite innovative designs, a large number of sensors have been rendered “bench top,” as the emphasis has been on the sensors, and the system (in particular the underlying embedded electronic system) has largely been ignored [11]. Only few tactile sensing arrays with electronic circuitry on chip with sensors have been presented so far. Those having any possess circuitry with minimal complexity, e.g., a single MOS transistor associated with each transducer.

To overcome the limits of current implementations, i.e. to design and develop large area tactile sensing arrays to be flexible, conformable, and stretchable and at the same time to be intimately integrated with the embedded electronic system and with functional (i.e. PVDF in our case) and structural materials, researchers need to address the development of *the tactile embedded electronic system* which intimately copes and integrates with technology and devices on one side and with system features and constraints on the other one.

The functions to be implemented by the *tactile embedded electronic system* are various and demand covering the whole signal chain: sensors biasing, signal conditioning (e.g. low noise amplification, low pass filtering, etc.), matrix readout, signal acquisition (i.e. Analog to Digital conversion), local digital signal processing, communication bus interface, etc. For instance one of the tasks of the tactile embedded electronic system is interfacing heterogeneous sensors, with different read out circuit modes, to the robot skin electronic infrastructure.

Based on the assessment of the sensing devices performance and on the system requirements, researchers need to address a proper and cost effective partitioning of the

tactile embedded electronic system between dedicated and COTS implementation. The design methodology and the partitioning must take into account the high number and types of sensors to be read, the high sampling bandwidth for some of them, the high expected data throughput, the limited communication bus bandwidth, the need for a low complexity implementation i.e. a small number of devices and interconnections, etc. Due to the complexity and diversity of tasks to be implemented, the digital core and part of the signal conditioning/data acquisition blocks need to be implemented by dedicated silicon electronic circuits (i.e. Application Specific Integrated Circuit, ASIC).

Dedicated communication strategies are needed to transmit the large amount of data (due to the high sampling rate as in the case of the PVDF sensors, i.e. at least 2 kSamples/s per sensor, and due to the large number of sensors in each array) collected by the tactile sensors arrays distributed over the whole body [31]. In this context, the hierarchical architecture of the communication bus and the local data processing (for a number of tasks e.g. feature extraction, data compression, etc.) is explored. Going from lower levels (i.e. skin) to higher levels (i.e. central processing unit) protocols are different. The desired operation speed, noise and number of wires put a constraint on the type of communication channel used for interaction with higher levels. Serial communication buses are used (e.g. I²C, Can bus, Flexray, Ethernet, etc.) to decrease wiring. The buses using CAN protocol are generally a preferred choice mostly due to the real-time capabilities, high reliability, and readily availability on most microcontrollers. But, the CAN bus suffers from a moderate transmission bandwidth (up to 1 Mbits/s) which will either slow down transmission of tactile data from a large number of sensors or put a cap on the number of touch sensors on the body. These issues can be solved either by using buses with higher transmission bandwidth (e.g. up to 10 Mbits/s can be achieved with FlexRay) or using more buses in parallel - which is anyway undesirable.

Due to the requirement of real time needed to use the tactile feedback in the control loop, deterministic protocols are mandatory. Going from periphery upwards, bandwidth of the bus increases in order to accommodate an increasing amount of data; protocol complexity increases as well. At lower levels high speed, lower connectivity and short distance wiring buses are preferred (e.g. I²C). Moving up in the hierarchy, more complex protocols and longer wiring buses are preferred (e.g. CAN, Flexray, real-time Ethernet like Ethercat).

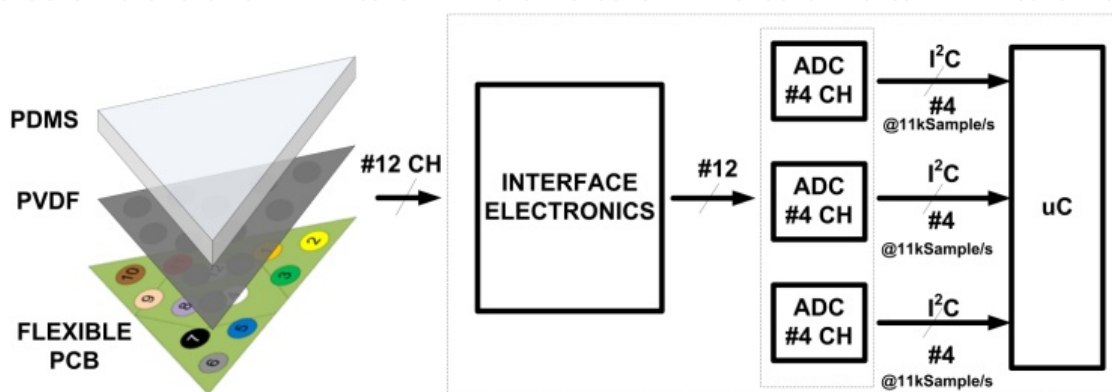


Figure 14. Block diagram of the system architecture with a triangle made of PVDF transducers.

The tactile sensing system based on PVDF transducer arrays proposed in this chapter [30] is based on a conformable mesh of sensor patches having a triangular shape [32]. On the bottom of the triangular substrate – which is in contact with the robot structure – the blocks of the interface and the local data acquisition/processing electronics are embedded (see Figure 14). The top surface hosts an array of 12 sensors/detectors covered by a PDMS protective layer. Each triangle is interconnected to each other to create a networked structure. Each patch is implemented on a flexible substrate allowing the system to conform to smooth curved surfaces of the robot body (i.e. upper limbs, torso, back, etc.). The PVDF film transducer is provided of two electrodes connected to wires which transfer the generated charge to the interface electronics. The PVDF sensor is used to detect tactile stimuli in the 1 Hz to 1 kHz range (corresponding to the human tactile sensing bandwidth). In the architecture shown in Figure 14, the 12 output signals from the triangle array are in input to the interface electronics (see Section 4). The interface electronics outputs the signals to three ADCs (MAX11613⁶) - each one manages 4 channels – and subsequently, through I²C buses, the signals are routed at 11kSample/s to the microcontroller (PIC24FJ64GB004 Family⁷). At present, skin patches (i.e. triangles) are interconnected through a CAN bus (the reference robotic platform is iCub⁸).

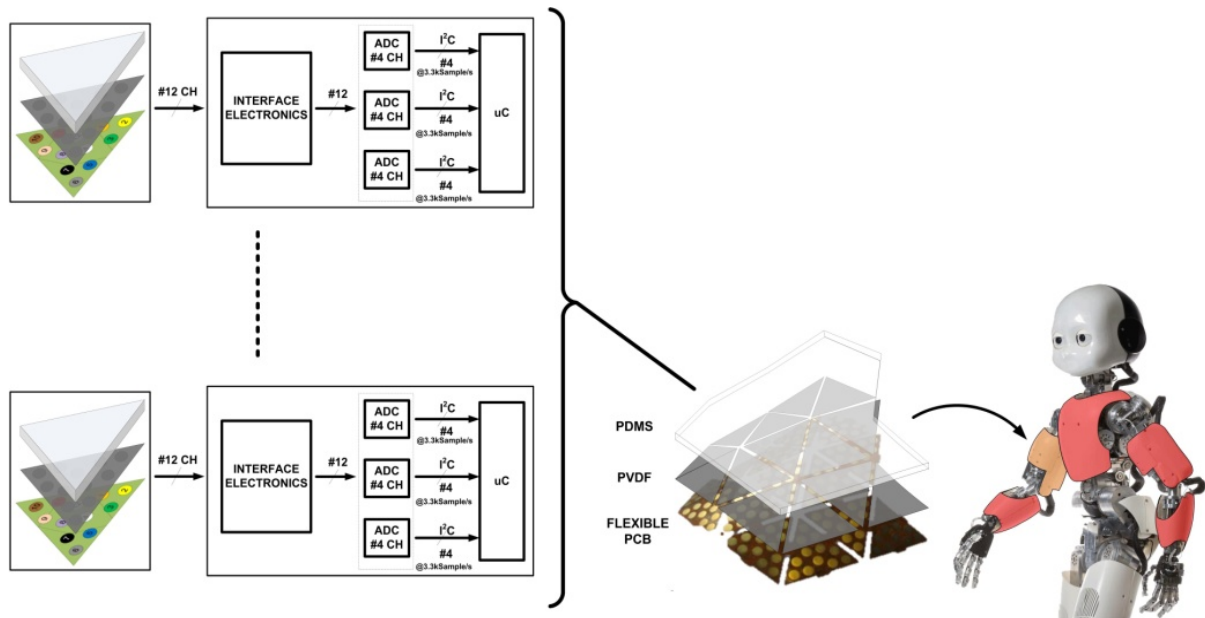


Figure 15. Tactile sensing system. iCub picture is printed by courtesy of IIT (Italian Institute of Technology).

⁶ <http://datasheets.maxim-ic.com/en/ds/MAX11612-MAX11617.pdf>

⁷ <http://ww1.microchip.com/downloads/en/devicedoc/39940c.pdf>

⁸ www.icub.org

To be able to integrate the interface and the data acquisition/local processing electronics onto the bottom of each triangle, and due to the small space available, an application-specific integrated circuit (ASIC), see Figure 15, which embeds: a) the interface electronics; b) data acquisition; c) dedicated signal processing; d) communication bus interface should be pursued. The feasibility and integration of the tactile sensing system on the robot will mainly depend on the design of the architecture of the ASIC.

7. Conclusions

The main objective of the research activity in this area is the design and manufacturing of robotic skin systems based on arrays of PVDF film transducers. We addressed issues concerning the manufacturing technology, the interface electronics and the system integration. The main achievements are summarized below.

The electromechanical characterization of PVDF thin films working in thickness mode has been achieved. The experimental d_{33} characterization shows a flat behavior in the whole range of frequencies of interest for the present application. Future steps would include the characterization of the PVDF tangential piezoelectric moduli and of the polymer behavior when used in bending mode. Another field of interest is related to the interpretation of PVDF creep and recovery following a step in load or temperature.

A number of elementary qualitative tactile perceptions have been experimentally quantified i.e. the corresponding mechanical contact force/stress have been evaluated. The contact pressure spans on about 5 orders of magnitude ranging from 50Pa to 5MPa. Achieved results complete relevant information in the latest literature about skin and perceived contacts. The contact stress/force range has been used as reference for the development of the interface electronics.

The PVDF transducer charge response to contact stresses has been evaluated in the defined range. We measured the charge response of a set of single taxel prototypes (i.e. PVDF thin film + cover layer) and we focused on gel/rubber layers excluding foams, to get more controllable and reproducible systems which also allow for the required dynamics. Measured charge spans over a range from about 0.01pC up to 1-2nC. The charge response results have been compared with an electromechanical model of the skin structure and have been used as reference specifications to design the interface electronics.

The interface electronics has been designed, implemented and tested. Experimental results validate the proposed solution in the frequency band of interest. The output signal ranges over three orders of magnitude. The experimental tests highlighted the need of a variable gain electronics solution to be able to measure the wide range of tactile stimuli expected for the application (i.e. 5 orders of magnitude for the expected mechanical stress due to contact).

The manufacturing technology for PVDF sensors arrays has been identified. In particular, the thickness (i.e. approximately 3mm) and material (PDMS) of the protective layer for the

triangular prototypes have been assessed and tested. Some prototypes of triangular sensor arrays have been manufactured and experimental results are encouraging. In this context, the next development is related to assess the reproducibility of the array behavior. Moreover, durability and calibration tests will be necessary to demonstrate the effective viability and reliability of the proposed technology.

A data processing algorithm for the estimation of the force distribution at the top surface of the covering layer is being currently investigated. Some additional work is however required, which is related to the optimization of the cost functional. Next step is toward the algorithm implementation into a dedicated embedded electronic system interfacing the tactile skin with the upper levels of the robot processing system. Once the force distribution has been obtained, the *Theorem of Work* can be employed to estimate the displacements at the surface of the elastomer. Extensions to non-parallel forces (torques, pinching and so on) and to large deflections are considered as next-future developments.

The system architecture (i.e. from the sensors arrays to the local microcontroller) has been identified. It is based on the following structure: PVDF sensor array (i.e. triangle), interface electronics (one for each channel), ADC converter with I²C communication interface, I²C bus, microcontroller.

Author details

Lucia Seminara and Luigi Pinna

Department of Biophysical and Electronic Engineering - University of Genoa, Italy

Maurizio Valle

Department of Biophysical and Electronic Engineering - University of Genoa, Italy

Research Center on Materials Science and Technology - University of Genoa, Italy

Marco Capurro

Research Center on Materials Science and Technology - University of Genoa

Department of Civil, Environmental and Architectural Engineering - University of Genoa, Italy

Acknowledgement

This work is supported by the ROBOSKIN European Project about “Skin-Based Technologies and Capabilities for Safe, Autonomous and Interactive Robots”, under grant agreement no. 231500.

8. References

- [1] Shimada M., Minato T., Itakura S., and Ishiguro H. (2007). Uncanny valley of androids and its lateral inhibition hypothesis. In Proc. IEEE International Symposium on Robot and Human interactive Communication, pp 374–379.

- [2] Breazeal, C. (2003). Toward sociable robots. *Robotics and Autonomous Systems*, 42:167–175.
- [3] Velonaki, M., Rye, D., Scheduling, S., and Williams, S. (2005). Fish-Bird: Autonomous interactions in a new media arts setting. In *Proc. Vital Signs: Creative Practice and New Media Now*, volume 29.
- [4] Robins, B, Dautenhahn K, Dubowski, J (2005) Robots as isolators or mediators for children with autism? A cautionary tale. *Proceedings of the AISB'05 Symposium on Robot Companions Hard Problems and Open Challenges in Human-Robot Interaction*, pp. 82-88.
- [5] Naya, F., Yamato, J., and Shinozawa, K. (1999). Recognizing human touching behaviors using a haptic interface for a pet-robot. In *Proc. IEEE International Conference on Systems, Man, and Cybernetics*, volume 2, pp 1030–1034.
- [6] Iwata, H. and Sugano, S. (2005). Human-robot-contact-state identification based on tactile recognition. *IEEE Transactions on Industrial Electronics*, 52(6):1468–1477.
- [7] Stiehl, W D, Lieberman, J, Breazeal, C, Basel, L, Lalla, L, Wolf, M (2005) Design of a Therapeutic Robotic Companion for Relational, Affective Touch. *Proceedings of the International Workshop on Robots and Human Interactive Communication*. pp. 408-415.
- [8] Koo, S., Lim, J. G., and Kwon, D. (2008). Online touch behavior recognition of hard-cover robot using temporal decision tree classifier. In *Proc. IEEE International Symposium on Robot and Human Interactive Communication*, pp 425–429.
- [9] Silvera Tawil, D., Rye, D., and Velonaki, M. (2011). Touch modality interpretation for an EIT-based sensitive skin. In *Proc. IEEE International Conference on Robotics and Automation*, pp. 3770–3776.
- [10] Lee, M, Nicholls, H (1999) Tactile sensing for mechatronics: A state of the art survey. *Mechatronics*. Vol. 9. No. 1: 1-31.
- [11] Dahiya, R S, Metta, G, Valle, M, Sandini, G (2010) Tactile Sensing: From Humans to Humanoids. *IEEE Transactions on Robotics*. 26 (1): 1-20.
- [12] Ohmura, Y., Kuniyoshi, Y., and Nagakubo, A. (2006). Conformable and scalable tactile sensor skin for curved surfaces. In *Proc. IEEE International Conference on Robotics and Automation*, pp. 1348–1353.
- [13] Um, D., Lumelsky, V. (1999). Fault tolerance via component redundancy for a modularized sensitive skin. In *Proceedings IEEE International Conference on Robotics and Automation*, v 1: 722-727
- [14] Tajika, T., Miyashita, T., Ishiguro, H. et al. (2006). Automatic Categorization of Haptic Interactions-What are the Typical Haptic Interactions Between a Human and a Robot. In *Proceeding of IEEE-RAS International Conference on Humanoid Robots, Humanoids 2006, Genova, 4-6 December 2006*.
- [15] Reston, R. and Kolesar, E. (1989). Pressure-sensitive field-effect transistor sensor array fabricated from a piezoelectric polyvinylidene fluoride film. In *Proc. Annual*

- International Conference of the IEEE Engineering in Medicine and Biology Society, 3: 918–919
- [16] Hosoda, K. (2003). Robot finger design for developmental tactile interaction: Anthropomorphic robotic soft fingertip with randomly distributed receptors. In Proc. Embodied Artificial Intelligence, 2865: 219–230.
- [17] Tanaka, Y., Tanaka, M., and Chonan, S. (2006). Development of a sensor system for measuring tactile sensation. In Proc. IEEE Conference on Sensors, pp. 554–557.
- [18] Dahiya, R., Valle, M., Metta, G., and Lorenzelli, L. (2007). POSFET tactile sensor arrays. In Proc. IEEE International Conference on Electronics, Circuits and Systems, pp. 1075–1078.
- [19] Ishiguro, H. and Nishio, S. (2007). Building artificial humans to understand humans. *Journal of Artificial Organs*, 10(3):133–142.
- [20] Takamuku, S., Gómez, G., Hosoda, K., and Pfeifer, R. (2007). Haptic discrimination of material properties by a robotic hand. In Proc. IEEE International Conference on Development and Learning, pp. 1–6.
- [21] Sandini, G, Maggiali, M, Cannata, G, Metta, G (2007) Tactile sensor arrangement and corresponding sensory system. United States Patent No. 20100234997.
- [22] E. R. Kandel, J. H. Schwartz, T. M. Jessell. *Principles of Neural Science*. McGraw-Hill/Appleton & Lange; 4th edition (January 5, 2000)
- [23] Mannsfeld, S.C.B., Tee B.C-K., Stoltenberg R.M., Chen C.V.H-H, Barman S., Muir B.V.O., Sokolov A.N., Reese C. and Bao Z. (2010). Highly sensitive flexible pressure sensors with microstructured rubber dielectric layers, *Nature Materials*, 9: 859–864
- [24] Ikeda, T (1996) *Fundamentals of Piezoelectricity*. Oxford Science Publications.
- [25] Seminara L, Capurro, M, Cirillo, P, Cannata, G, Valle, M (2011) Electromechanical characterization of piezoelectric PVDF polymer films for tactile sensors in robotics applications. *Sens. Actuators A*. 169 (1): 49-58.
- [26] Vinogradov, A M, Holloway F (1999) Electro-mechanical properties of the piezoelectric polymer PVDF. *Ferroelectrics*, 226: 169-181.
- [27] Johnson, K.L. (1985). Description of Contact Mechanics and Boussinesq equation in elastic surface, in *Contact Mechanics*, Cambridge University Press, New York, NY.
- [28] Selvadurai A.P.S. (2001). On Boussinesq's problem. *International Journal of Engineering Science*, 39: 317-322
- [29] Albert, A (1972) *Regression and the Moore-Penrose pseudoinverse*. Academic Press Ink. New York.
- [30] Pinna, L, Carlini, G, Seminara, L, Valle, M (2011) Interface electronics for tactile sensing arrays. *Electronics, Circuits and Systems (ICECS)*, 2011. 18th IEEE International Conference on. pp. 468-471.
- [31] Ravinder, R S, Valle, M (2012) *Robotic Tactile Sensing – The Silicon way to System*. Elsevier Publishing.

- [32] Cannata, G, Maggiali, M, Metta, G, Sandini, G (2008) An embedded artificial skin for humanoid robots. IEEE International Conference on Multisensor Fusion and Integration for Intelligent Systems, 2008. MFI 2008. pp. 434-438.

IntechOpen

IntechOpen